A TENTATIVE DETECTION OF AN EMISSION LINE AT 1.6 μm FOR THE $z \sim 12$ CANDIDATE UDFj-39546284[*]

Gabriel B. Brammer[1], Pieter G. van Dokkum[2], Garth D. Illingworth[3], Rychard J. Bouwens[4],
Ivo Labbé[4], Marijn Franx[4], Ivelina Momcheva[2], and Pascal A. Oesch[3]
[1] European Southern Observatory, Alonso de Córdova 3107, Casilla 19001, Vitacura, Santiago, Chile; gbrammer@eso.org
[2] Department of Astronomy, Yale University, New Haven, CT 06520, USA
[3] UCO/Lick Observatory, University of California, Santa Cruz, CA 95064, USA
[4] Leiden Observatory, Leiden University, NL-2300 RA Leiden, The Netherlands

ABSTRACT

We present deep WFC3 grism observations of the candidate $z \sim 12$ galaxy UDFj-39546284 in the *Hubble Space Telescope* (*HST*) Ultra Deep Field (UDF), by combining spectroscopic data from the 3D-HST and CANDELS surveys. The total exposure time is 40.5 ks and the spectrum covers $1.10 < \lambda < 1.65\,\mu$m. We search for faint emission lines by cross-correlating the two-dimensional G141 spectrum with the observed H_{160} morphology, a technique that is unique to slitless spectroscopy at *HST* resolution. We find a 2.7σ detection of an emission line at 1.599 μm—just redward of the JH_{140} filter—with flux $3.5 \pm 1.3 \times 10^{-18}$ erg s^{-1} cm^{-2}. Assuming that the line is real, it contributes $110\% \pm 40\%$ of the observed H_{160} flux and has an observed equivalent width >7300 Å. If the line is confirmed, it could be Lyα at $z = 12.12$. However, a more plausible interpretation, given current results, could be a lower redshift feature such as [O III]λ4959,5007 at $z = 2.19$. We find two other 3D-HST [O III] emitters within 1000 km s^{-1} of that redshift in the GOODS-South field. Additional support for this interpretation comes from the discovery of a bright "[O III] blob" with a secure G141 grism redshift of $z = 1.605$. This object has a strikingly large observed equivalent width of nearly 9000 Å that results in similar "dropout" colors as UDFj-39546284.

Key words: galaxies: formation – galaxies: high-redshift

Online-only material: color figures

1. INTRODUCTION

Over the past few years deep imaging programs with the WFC3 camera on the *Hubble Space Telescope* (*HST*) have opened up the universe at $z > 8$ for systematic study (e.g., Bouwens et al. 2011a, 2012a; Oesch et al. 2012; Ellis et al. 2013; Coe et al. 2013). Photometric data can provide strong constraints on the redshifts and properties of very high-redshift galaxies (e.g., Bouwens et al. 2011b, 2012b). However, the interpretation is hampered by the lack of spectroscopic information that provides unambiguous redshift determination and the contributions of emission lines to the broadband fluxes. The equivalent widths of rest-frame optical lines increase with redshift (e.g., Fumagalli et al. 2012), and the emission-line contribution can be significant even in the broad Infrared Array Camera filters (e.g., Labbé et al. 2010; Ono et al. 2010).

Obtaining high-quality spectra of these very distant objects is a formidable challenge because of their faintness and because key emission and absorption features are redshifted into the observer's near-IR. Apart from a gamma-ray burst at $z = 8.1$ (Salvaterra et al. 2009; Tanvir et al. 2009) the only claimed (and disputed; Bunker et al. 2013) detection is an Lyα line at $z = 8.6$ in a z-dropout galaxy in the Ultra Deep Field (UDF; Lehnert et al. 2010).

Here we describe a deep WFC3 G141 grism spectrum of one of the most intriguing high-redshift candidates yet discovered: UDFj-39546284. This object was identified as the first robust $z \gtrsim 10$ candidate by Bouwens et al. (2011a): it was only detected in H_{160} in the HUDF09 data set (see also Oesch et al. 2012). Recent observations from the HUDF12 program (Ellis et al. 2013) confirm the H_{160} detection and show that it is undetected

in JH_{140} (Ellis et al. 2013; Bouwens et al. 2013). The >1.4 mag dropout (2σ) in the JH_{140} filter pushes its likely redshift to $z \sim 12$, although alternative explanations cannot be ruled out (Ellis et al. 2013). Here we report a 2.7σ detection of an emission line for UDFj-39546284 that would account for most or all of its H_{160} flux. Though this line could be Lyα at $z = 12$, we argue that it is more likely to be [O III]λ4959,5007 at $z = 2.19$ based in part on the discovery of a bright low-redshift analog with one of the highest [O III] equivalent widths ever observed (8700 Å) and broadband colors similar to UDFj-39546284. Magnitudes are in the AB system throughout.

2. OBSERVATIONS AND ANALYSIS

The UDF was observed with the WFC3/G141 grism as part of the 3D-HST survey (GO-12177; PI: van Dokkum; Brammer et al. 2012a). The observations comprise four separate visits at the same orientation with G141 integrations of 4.7 ks (two orbits) each. The UDF was also observed by the CANDELS supernova follow-up program (GO-12099, PI: Riess) when a supernova at $z = 1.55$, nicknamed "Primo," was discovered in the first epoch of CANDELS imaging in the GOODS-South field (see Rodney et al. 2012). The field was observed in two visits on 2010 October 26 and 2010 November 01 with G141 integrations of 6.6 and 15 ks, respectively. The position angle of the grism dispersion axis is rotated by 6°.4 between the two visits, which together are rotated 50° with respect to the 3D-HST visits. The relation of the G141 pointings to the deep HUDF09+HUDF12 imaging area is shown in Figure 1.

The Primo and 3D-HST visits were pre-processed separately and identically using the `threedhst` pipeline[5] (Brammer et al. 2012a). The individual exposures of each visit were then combined into a mosaic by interlacing the pixels to a subgrid

---

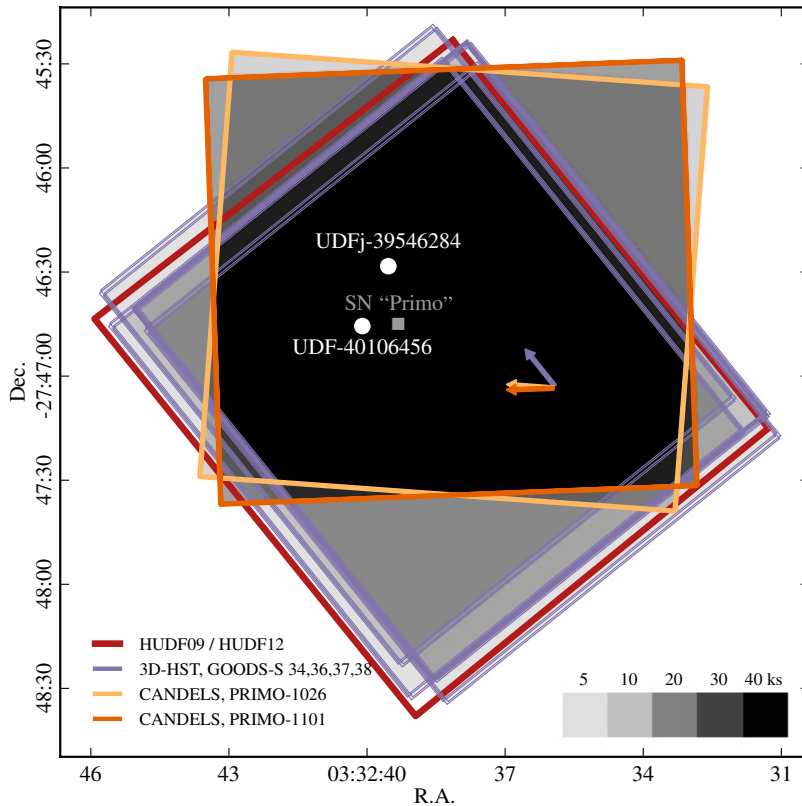[5] http://code.google.com/p/threedhst/

Figure 1. Exposure map of the 3D-HST and CANDELS G141 grism pointings in the HUDF. The vectors indicate the direction and extent of the first-order G141 spectra. The locations of the CANDELS supernova and the two faint UDF galaxies described below are indicated. These objects lie in the area of deepest G141 grism coverage, with a total exposure time of 40.5 ks (17 orbits).

(A color version of this figure is available in the online journal.)

of pixels that are exactly half their original size. Interlacing pixels from input images that have 0.5 pixel offsets (by design in 3D-HST and rounded for CANDELS-Primo) results in a one-to-one correspondence between input and output pixels (e.g., van Dokkum et al. 2000) and offers the key benefit of preserving the individual pixel errors.

With the HUDF12 H_{160} image defining the 1.6 μm flux densities and spatial morphologies, we compute a full quantitative contamination model of all objects in the field to $H_{160} < 28$. The modeling technique, first presented in Brammer et al. (2012b), includes the first four spectral orders, among them the compact zeroth order that can resemble emission lines. The models of bright objects with $H_{160} < 23$ are refined based on their observed spectra, while fainter objects are assumed to have continua flat in units of f_λ. Therefore, emission lines in fainter galaxies are not included in the contamination model.

To generate a deep two-dimensional (2D) spectrum from all UDF grism integrations, we first extract 2D spectra from each visit. These spectra are aligned in two dimensions to the nearest pixel in the subsampled grid and the aligned pixels are then combined with inverse variance weights including a term to down-weight contaminated pixels. Stacked spectra from the central 3 arcmin^2 of the UDF have a combined exposure time of 40.5 ks.

3. A TENTATIVE EMISSION LINE IN UDFj-39546284

3.1. The Deep Near-IR Spectrum

The 2D 40.5 ks G141 spectrum of UDFj-39546284 is shown in Figure 2. While some contamination remains in the stacked spectrum, the orientations of the UDF/G141 visits turn out to

be nearly perfect for avoiding significant contamination of the UDFj-39546284 spectrum, particularly at $\lambda > 1.4\,\mu$m. The contamination-subtracted spectrum is remarkably clean with none of the systematics that typically plague ground-based NIR spectroscopy (see, e.g., Lehnert et al. 2010). The cluster of bright pixels at the top of the spectrum is likely a faint contaminant emission line not included in the model; it lies well away from any contribution from UDFj-39546284.

The "salt-and-pepper" appearance of the 2D spectrum is the result of the uncorrelated noise of the individual pixels. The distribution of cleaned pixel values is Gaussian with $\sigma_{\rm obs} = 0.0033$ electrons s^{-1}. Random Gaussian deviates scaled by the propagated pixel errors have $\sigma_{\rm err} = 0.0036$ electrons s^{-1}. This slight overestimation of the errors by 10% is significantly lower than the factors of 60%–70% that result from typical applications of the Drizzle algorithm (Fruchter et al. 2009).

3.2. A 2σ Emission-line Detection at λ = 1.599 μm

Slitless *HST* grism spectra offer a distinct advantage compared to ground-based data for detecting weak emission-line features: the 2D spectrum provides an image of the galaxy at the wavelength of the emission line (see, e.g., Brammer et al. 2012b), and the morphology of the galaxy is known a priori from the deep broadband WFC3 imaging. As long as the emission-line morphology and the broadband morphology are similar (which is generally the case at $z \sim 1$; Nelson et al. 2012), or the line contributes significantly to the broadband flux (which is the case here; see below), we can search for features in the 2D spectrum whose morphology corresponds to that of the broadband image.
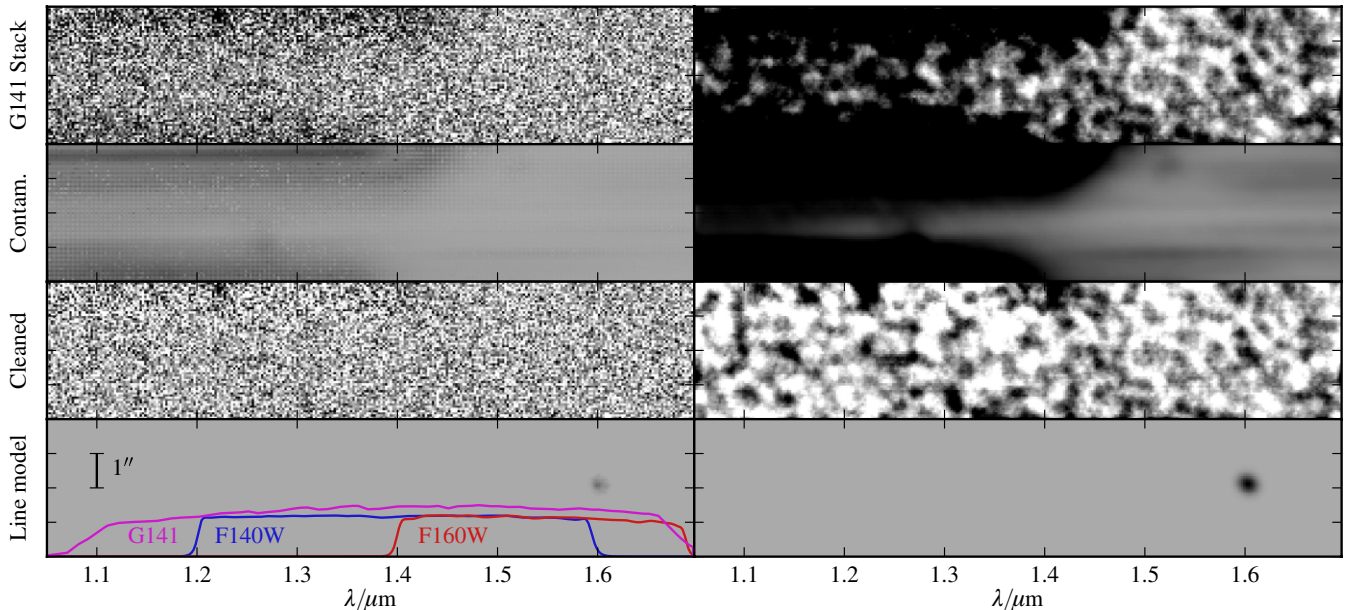
Figure 2. Deep G141 grism spectrum of UDFj-39546284. The left panels show the pixels as observed and modeled, and the right panels show the spectra cross-correlated with the H_{160} object profile to enhance weak features. The first row shows the stacked spectrum as observed. The second row shows the contamination model (Section 2), with some aliasing due to the unequal weights of the interlaced Primo mosaics. The third row shows the observed spectrum cleaned of this contamination. There is a weak emission feature in the cross-correlation spectrum at $\lambda = 1.599\,\mu$m. The bottom row shows the emission-line model of UDFj-39546284 where the morphology is derived from the observed H_{160} image (see also Figure 3).

(A color version of this figure is available in the online journal.)

While there are no obvious emission lines in the raw 2D spectrum, there is a clump of pixels at $\sim 1.6\,\mu$m which is marginally enhanced compared to its surroundings. To improve the signal-to-noise (S/N) of this feature, we cross-correlate the 2D spectrum with a kernel defined by the central $R = 0\farcs3$ of the deep H_{160} thumbnail of UDFj-39546284. This kernel is constructed by extracting kernels for each of the individual UDF/G141 visits with different orientations and combining them weighting by the median error in their corresponding 2D grism spectra. Thus, the object profile is slightly smoothed but will reflect the 2D morphology of lines in the stacked spectrum. The cross-correlation spectrum is shown in the right-hand panels of Figure 2, and the strength of the feature at $1.6\,\mu$m is enhanced compared to the raw 2D spectrum. We verified that the weak feature is not visible in a similar analysis of any single UDF/G141 visit, confirming that the feature does not arise from a flux excess in one of them individually, such as a group of hot pixels or an unflagged cosmic ray.

We show a one-dimensional spectrum extracted along the trace in Figure 3. We compute an associated uncertainty at each pixel along the trace, highlighted in blue, by cross-correlating the squared error array with the same H_{160} kernel. Furthermore, we compute a 2D model spectrum as in Figure 2 with known position and integrated line flux, and extract its cross-correlation spectrum in the same way as the observed spectrum. The feature at $\lambda = 1.599 \pm 0.004\,\mu$m is detected at 2.7σ with an integrated line flux of $3.5 \pm 1.3 \times 10^{-18}\,$erg s^{-1} cm^{-2}. The probability of finding a Gaussian noise feature with equal or greater significance is $\sim 10\%$ for 30 independent resolution elements ($\sim 3000\,$Å).

3.3. The Reality of the 1.599 μm Feature

There are regions in the 2D cross-correlation spectrum with apparently similar significance to the feature at $1.6\,\mu$m. Many of them can be rejected because they do not fall precisely along

the trace of the grism spectrum. There are enhancements found near the trace at $\lambda = 1.14\,\mu$m and $1.22\,\mu$m, though these wavelengths suffer from higher contamination perhaps consisting of faint emission lines not included in the contamination model. The *HST*/WFC3 broadband photometry places strong constraints on the possibility that these lines come from UDFj-39546284: either of the bluer lines alone would result in Y_{105} or J_{125} two magnitudes brighter than the 2σ HUDF12 limits.

In contrast, the $1.599\,\mu$m line is consistent with the HUDF12 photometry. Within the same $0\farcs3$ aperture used to measure the line flux, we measure $H_{160} = 29.04$ for the H_{160} kernel. This is 27% brighter than the Ellis et al. (2013) magnitude measured within an $0\farcs25$ aperture, but is only 73% of the total magnitude measured by Bouwens et al. (2013). These differences are consistent with aperture corrections of the extended source, which shows a faint extended tail to the NE in the H_{160} image (Bouwens et al. 2013). A pure emission line with the observed flux would result in $H_{160} = 28.92$; the line accounts for $110\% \pm 40\%$ (1σ) of the H_{160} flux. This corresponds to a $(1, 2)\sigma$ limit on the observed-frame equivalent width of the line of EW $> (7300, 1300)$ Å.

We test our technique by analyzing faint lines of another UDF galaxy with a secure redshift, UDF-40106456 (right panels of Figure 3). This galaxy has $H_{160} = 27.4$ and unambiguous emission lines of Hα and [O III]λ4959,5007 at $z = 1.303$ visible in the stacked 2D spectrum before cross-correlation. Using the cross-correlation technique we find a significant detection of Hβ even though the line is barely visible in the original spectrum. Two spurious features are detected at $1.24\,\mu$m and $1.29\,\mu$m with comparable flux as the tentative line in UDFj-39546284. These are both clearly associated with residual contamination from another source at the top of the 2D spectrum. The Hα line flux of UDF-40106456 is $9.5 \pm 1.0 \times 10^{-18}\,$erg s^{-1} cm^{-2}, just three times brighter than the UDFj-39546284 emission line. The detection significance is S/N ~ 10 and the
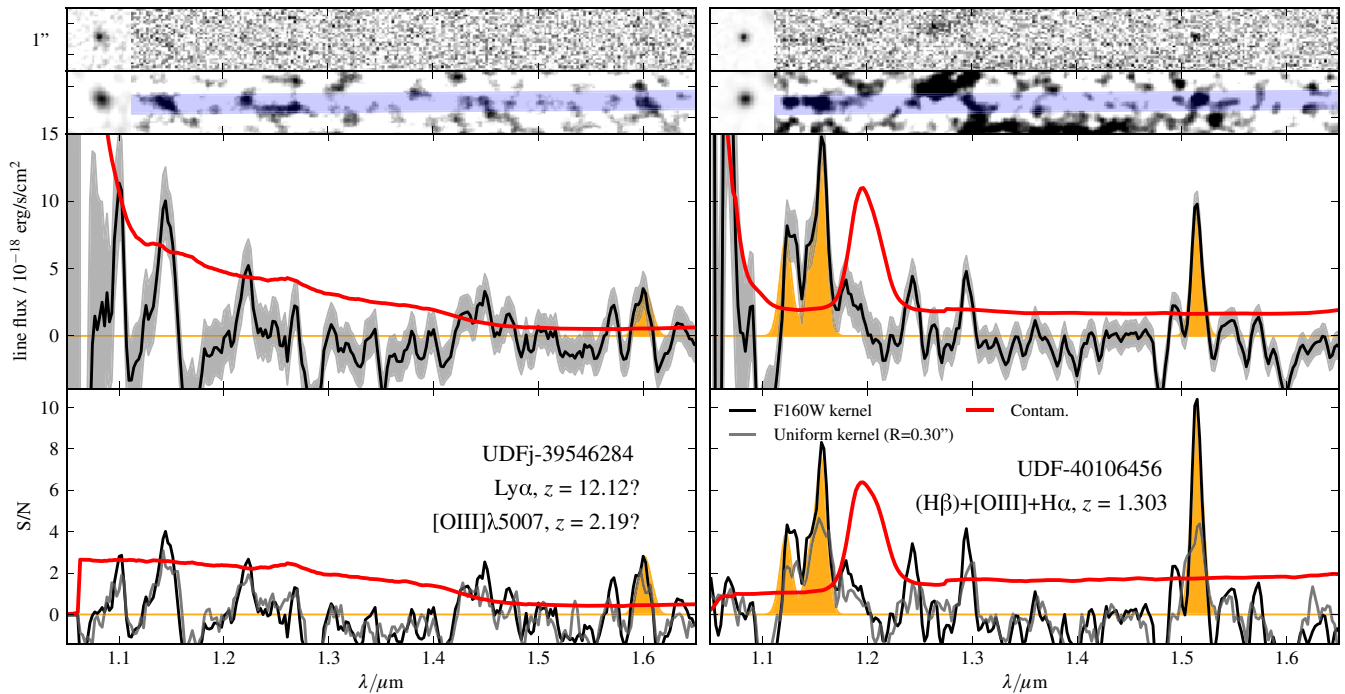
Figure 3. Optimal extraction of the UDFj-39546284 spectrum (left) and that of a comparison object, UDF-40106456 (right). The top panels show the stacked 2D spectra and the spectra cross-correlated with the H_{160} image kernel, which is indicated at left. The upper spectra show the 2D cross-correlation extracted along the trace and scaled by the G141 sensitivity curve and $\Delta\lambda$ of the spectrum, which, for a uniform kernel, would give an integrated line flux with the units as labeled. The same cross-correlation is applied to the 2D pixel variance array, yielding the uncertainties shaded in gray. The bottom panels show the signal-to-noise spectrum. While there are additional apparently significant features at $\lambda < 1.5\,\mu$m, these are likely due to contamination rather than coming from UDFj-39546284 (Section 3.3). The gray curves in the bottom panels show the S/N in $R = 0\farcs3$ apertures along the trace. The red curves indicate the potential contamination from nearby sources. The filled orange regions are model emission-line spectra, whose shapes match those of the observed lines.

(A color version of this figure is available in the online journal.)

cross-correlation technique enhances the detection significance by a factor of two compared to simple photometry along the trace within an equivalent $0\farcs30$ aperture. This example demonstrates that the cross-correlation technique works and is able to recover extremely faint emission lines.

4. LINE IDENTIFICATION

4.1. Is UDFj-39546284 at $z = 12$?

If the galaxy is at $z \sim 12$, as is suggested based on its strong photometric break between the JH_{140} and H_{160} filters (Ellis et al. 2013; Bouwens et al. 2013), the line—if real—can be identified as Lyα redshifted to $z = 12.12$. The rest-frame equivalent width of Lyα would not be unreasonably high at >170 Å (accounting for the $z = 12$ Lyman break in H_{160}); such values can be reached in young, low-metallicity starbursts at high redshift (Schaerer 2003). However, such strong Lyα emission might be unexpected early in the reionization epoch when the neutral fraction is high (Santos 2004; but see also Dijkstra et al. 2011). More to the point, if the line is real it can account for most or all of the H_{160} flux, meaning that the photometric break does not necessarily reflect a strong continuum break and the photometric redshift is unreliable. Therefore, the line could also be a longer-wavelength feature at much lower redshift, a possibility discussed by Ellis et al. (2013).

4.2. Low-redshift Solutions—[O III] at $z = 2.2$

Although we cannot exclude other low-redshift identifications such as [O II] at $z = 3.28$ or Hα at $z = 1.44$, a likely possibility is that the line is [O III]λ4959,5007 at $z = 2.19 \pm 0.01$. A

population of extreme [O III] emission-line galaxies at $z \sim 1.7$ was recently identified by van der Wel et al. (2011) from their significant line contribution to the J_{125} photometry in the CANDELS survey. Additional galaxies with [O III] rest-frame equivalent widths reaching 2000 Å have been identified in WFC3 grism spectroscopy by Atek et al. (2011) and Brammer et al. (2012b). The strongest emitters in van der Wel et al. (2011) have $J_{125} - H_{160} \sim -1$, with [O III] in the J_{125} band. While such colors can mimic those of high-redshift dropout galaxies (Atek et al. 2011), even more extreme equivalent widths at $\gtrsim 3000$ Å (rest frame) are required to reach $J_{125/140} - H_{160} > 1.4$ observed for UDFj-39546284.

4.3. Discovery of a Possible Analog: An Extreme [O III] Emitter at $z = 1.605$

We have discovered a very bright example of such an extreme emission-line galaxy in G141 grism observations of the Extended Groth Strip (EGS) field (GO-12547, PI: Cooper). This remarkable object, EGS-XEW-1, located at $\alpha = 14$:17:58.2, $\delta = +52$:31:35 and shown in Figure 4, is an "[O III] blob" at $z = 1.605$ with $JH_{140} = 21.5$ and a complex morphology comprised of diffuse (A) and compact (B) components separated by $1''$. The exposure times and dithered pixel sampling for the Cooper et al. grism program are nearly identical to those of 3D-HST, and the spectra were processed with the 3D-HST interlacing software as described above. The diffuse component, which is extended over more than $1''$ (8.5 kpc), has a combined observed-frame equivalent width of nearly 9000 Å for the blended Hβ and [O III]λ4959,5007 emission lines. The more compact component has EW = 3000 ± 160 Å.
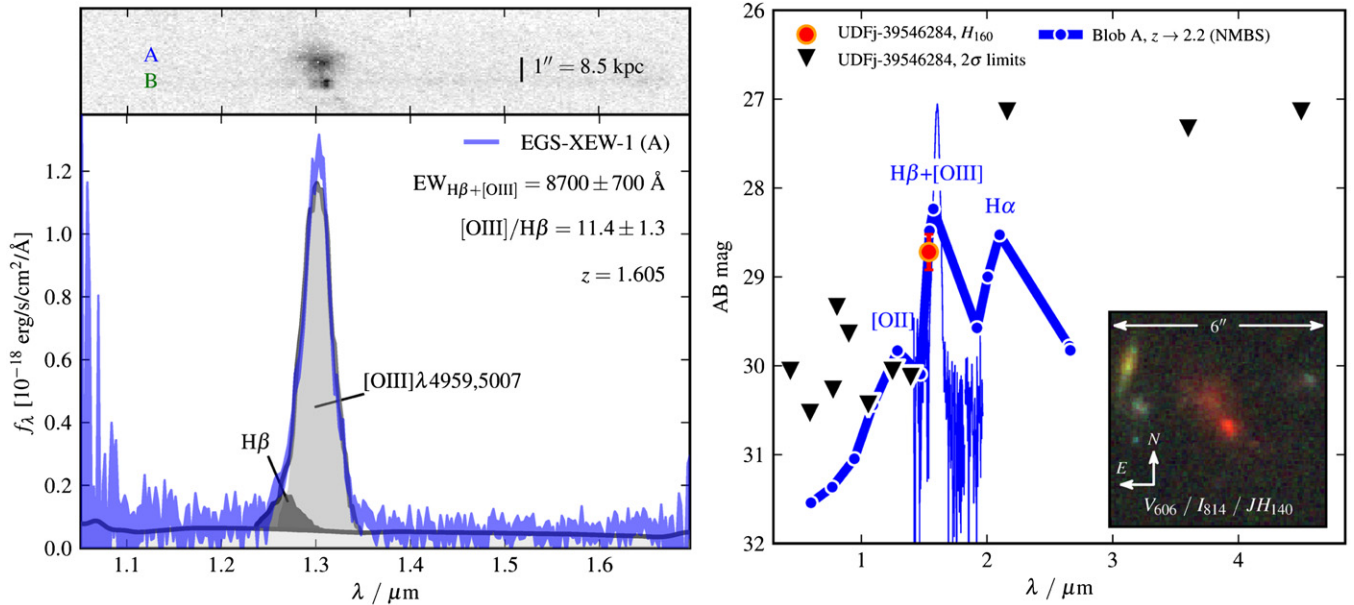
Figure 4. WFC3/G141 spectrum and broadband SED of EGS-XEW-1, an "[O III] blob" at $z = 1.605$ with extreme [O III] emission lines and colors similar to UDFj-39546284. The asymmetric line profile of component A is consistent with lines of Hβ and the [O III]λ4959,5007 doublet as indicated; the lines are unambiguously resolved for component B, at the same redshift. The right panel shows the SED of the blob normalized to that of the UDFj-39546284 H_{160} magnitude. Non-detections for UDFj-39546284 are shown with 2σ upper limits taken from Bouwens et al. (2013). Along with the G141 spectrum, ground-based photometry of the blob from the NEWIRM Medium Band Survey (NMBS) (Whitaker et al. 2011) is shown in blue, redshifted such that the [O III] line would have been observed at 1.6 μm and scaled to account for the different NMBS-J3, JH_{140}, and H_{160} passbands. The inset shows a color thumbnail of the blob created from *HST* ACS/V_{606}, ACS/I_{814}, and WFC3/JH_{140} images.

(A color version of this figure is available in the online journal.)

The broadband spectral energy distribution (SED) of EGS-XEW-1 is compared to that of UDFj-39546284 in the right panel of Figure 4. The spectral break that results from a line such as the one observed in EGS-XEW-1 is just large enough to satisfy the 2σ limit on the $JH_{140} - H_{160}$ dropout color of UDFj-39546284. However, if UDFj-39546284 had exactly the same spectrum as EGS-XEW-1, the [O II]λ3727 line would probably be detected in the bluer WFC3 HUDF12 photometry. Interestingly, EGS-XEW-1 has much redder UV colors than $f_\lambda \sim \lambda^{-2}$ observed for the high equivalent width starbursts at similar redshifts (van der Wel et al. 2011; Brammer et al. 2012b), which, if also true for UDFj-39546284, could help explain the lack of $z = 2$ Lyα observed for that source (Ellis et al. 2013). While not a perfect match, EGS-XEW-1 provides a directly observed route to a plausible low-redshift interpretation for the UDFj-39546284 photometry.

5. DISCUSSION AND CONCLUSIONS

We have described a deep *HST* grism spectrum of the candidate $z = 12$ galaxy UDFj-39546284. Using the known emission-line morphology to increase the line sensitivity of the slitless grism spectrum, we detect a tentative emission line at $\lambda = 1.599\,\mu$m with flux $3.5 \pm 1.3 \times 10^{-18}\,\mathrm{erg\,s^{-1}\,cm^{-2}}$ and observed-frame equivalent width >7300 Å.

While the current observations do not conclusively forbid the $z = 12$ interpretation of UDFj-39546284, a number of independent factors conspire to suggest that the 2.7σ line is in fact real and that the true redshift of UDFj-39546284 is $z \sim 2.2$. First, the line is observed at just the right wavelength and flux to satisfy both the HUDF H_{160} detection and the >1.4 mag dropout at $\lambda < 1.595\,\mu$m in the bluer *HST* bands. If the feature were observed just 4 pixel (93 Å) bluer it would violate the constraints on JH_{140} by a magnitude. Second, Bouwens et al.

(2013) demonstrate that without a significant contribution of Lyα to the H_{160} flux, the implied rest-frame UV luminosity for $z \sim 12$ is some 20 times higher than would be expected from the evolution of the luminosity function at $z = 8$–10. Third, recent deep spectroscopic surveys of photometric dropouts find a decreasing fraction of Lyα emitters with increasing redshift when the universe was increasingly neutral (Pentericci et al. 2011; Caruana et al. 2012). Fourth, we show that spatially extended objects with EW > 7300 Å exist at $z \sim 2$. Finally, we find at least two [O III] emitters within 1000 km s^{-1} of the $z = 2.19$ solution for UDFj-39546284 in the 3D-HST coverage of the full GOODS-South field, the nearest separated by 69″ (570 kpc); the fact that other galaxies exist at this exact redshift increases the probability that the line is real and is [O III]λ4959,5007.

If the physical properties of UDFj-39546284 are similar to either the [O III] blob EGS-XEW-1 or to the high equivalent width starbursting dwarf galaxies studied by van der Wel et al. (2011), UDFj-39546284 at $z = 2.2$ would represent a new class of object 750 times fainter than the former or $\sim$30 times fainter than the latter. Scaling from the typical stellar masses of the van der Wel et al. (2011) galaxies, UDFj-39546284 would have a stellar mass of the order of $10^6\,M_\odot$, similar to the mass of a single massive star cluster (e.g., Reines et al. 2008). The extended H_{160} morphology would then indicate the distribution of ionized gas surrounding the cluster.

The most urgent question is whether the line is real and associated with UDFj-39546284 as opposed to coming from a nearby contaminating object spectrum or simply being a clump of positive noise fluctuations. If the line is real and is [O III] at $z = 2.2$, it should be possible to detect the 4959 and 5007 Å lines of the doublet separately, either in (much) deeper grism data or in deep ground-based spectroscopy. Hα may also be visible in the K band at a similar flux as [O III] (Figure 4).

Regardless of the reality of the emission line, we have shown that the broadband SED of UDFj-39546284 provides a reasonable match to a low-redshift SED, specifically the *observed* spectrum of EGS-XEW-1, an "[O III] blob" at $z = 1.605$, redshifted to $z = 2.2$. This study demonstrates that the G141 grism on WFC3 can provide clean spectra with well-understood noise properties in deep integrations up to at least 40 ks (17 orbits).

REFERENCES

Atek, H., Siana, B., Scarlata, C., et al. 2011, ApJ, 743, 121
Bouwens, R., Bradley, L., Zitrin, A., et al. 2012a, arXiv:1211.2230
Bouwens, R. J., Illingworth, G. D., Labbe, I., et al. 2011a, Natur, 469, 504
Bouwens, R. J., Illingworth, G. D., Oesch, P. A., et al. 2012b, ApJ, 754, 83
Bouwens, R. J., Illingworth, G. D., Oesch, P. A., et al. 2011b, ApJ, 737, 90
Bouwens, R. J., Oesch, P. A., Illingworth, G. D., et al. 2013, ApJL, in press (arXiv:1211.3105)
Brammer, G. B., Sánchez-Janssen, R., Labbé, I., et al. 2012b, ApJL, 758, L17
Brammer, G. B., van Dokkum, P. G., Franx, M., et al. 2012a, ApJS, 200, 13
Bunker, A. J., Caruana, J., Wilkins, S. M., et al. 2013, MNRAS, in press (arXiv:1301.4477)
Caruana, J., Bunker, A. J., Wilkins, S. M., et al. 2012, MNRAS, 427, 3055
Coe, D., Zitrin, A., Carrasco, M., et al. 2013, ApJ, 762, 32
Dijkstra, M., Mesinger, A., & Wyithe, J. S. B. 2011, MNRAS, 414, 2139
Ellis, R. S., McLure, R. J., Dunlop, J. S., et al. 2013, ApJL, 763, L7
Fruchter, A., Sosey, M., Hack, W., et al. 2009, The MultiDrizzle Handbook, v3.0, Technical Report, http://www.stsci.edu/hst/HST_overview/documents/multidrizzle
Fumagalli, M., Patel, S. G., Franx, M., et al. 2012, ApJL, 757, L22
Labbé, I., González, V., Bouwens, R. J., et al. 2010, ApJL, 716, L103
Lehnert, M. D., Nesvadba, N. P. H., Cuby, J.-G., et al. 2010, Natur, 467, 940
Nelson, E. J., van Dokkum, P. G., Brammer, G., et al. 2012, ApJL, 747, L28
Oesch, P. A., Bouwens, R. J., Illingworth, G. D., et al. 2012, ApJ, 745, 110
Ono, Y., Ouchi, M., Shimasaku, K., et al. 2010, ApJ, 724, 1524
Pentericci, L., Fontana, A., Vanzella, E., et al. 2011, ApJ, 743, 132
Reines, A. E., Johnson, K. E., & Hunt, L. K. 2008, AJ, 136, 1415
Rodney, S. A., Riess, A. G., Dahlen, T., et al. 2012, ApJ, 746, 5
Salvaterra, R., Della Valle, M., Campana, S., et al. 2009, Natur, 461, 1258
Santos, M. R. 2004, MNRAS, 349, 1137
Schaerer, D. 2003, A&A, 397, 527
Tanvir, N. R., Fox, D. B., Levan, A. J., et al. 2009, Natur, 461, 1254
van der Wel, A., Straughn, A. N., Rix, H.-W., et al. 2011, ApJ, 742, 111
van Dokkum, P. G., Franx, M., Fabricant, D., et al. 2000, ApJ, 541, 95
Whitaker, K. E., Labbé, I., van Dokkum, P. G., et al. 2011, ApJ, 735, 86